Chromatin compaction and spatial organization in rice interphase nuclei

Alžběta Doležalová[1], Denisa Beránková[1], Veronika Koláčková[1], Eva Hřibová[1*]

[1] Institute of Experimental Botany of the Czech Academy of Sciences, Centre of Plant Structural and Functional Genomics, 77900 Olomouc, Czech Republic

Short title: Chromatin compaction and spatial organization in rice

*Corresponding Author:
Eva Hřibová
Institute of Experimental Botany
Šlechtitelů 31
779 00 Olomouc
Czech Republic
Tel: +420 585 238 713
E-mail:hribova@ueb.cas.cz

E-mail addresses:
Doležalová A. - dolezalova@ueb.cas.cz
Beránková D. - berankova@ueb.cas.cz
Koláčková V. - kolackova@ueb.cas.cz

Highlight

Super-resolution STED microscopy uncovered detailed chromatin ultrastructure; high level of differences in chromatin condensation and mutual positioning of chromosome territories between and within leaf and root meristem G1 were observed.

Abstract

Chromatin organization and its interactions are essential for biological processes such as DNA repair, transcription, and DNA replication. Detailed cytogenetics data on chromatin conformation, and the arrangement and mutual positioning of chromosome territories in

interphase nuclei are still widely missing in plants. In this study, level of chromatin condensation in interphase nuclei of rice (*Oryza sativa*) and the distribution of chromosome territories (CTs) were analyzed. Super-resolution, stimulated emission depletion (STED), microscopy showed different level of chromatin condensation in leaf and root interphase nuclei. 3D immuno-FISH experiments with painting probes specific to chromosomes 9 and 2 were conducted to investigate their spatial distribution in root and leaf nuclei. Six different configurations of chromosome territories, including their complete association, weak association, and complete separation, were observed in root meristematic nuclei, and four configurations were observed in leaf nuclei. The volume of CTs and frequency of their association varied between the tissue types. The frequency of association of CTs specific to chromosome 9, containing NOR region, is also affected by the activity of the 45S rDNA locus. Our data suggested that the arrangement of chromosomes in the nucleus is connected to the position and the size of the nucleolus.

Introduction

Nuclear DNA is condensed together with structural proteins into higher-order chromatin structures, which serve as substrates for important biological processes such as DNA replication, transcription, and genome repair (Misteli, 2020). While the chromatin is packed into visible, highly condensed chromosome structures during mitosis, it is decondensed in the interphase of the cell cycle, and the borders of individual chromosomes can not be recognized. The fundamental questions are: how is the chromatin packed into chromosomes, how are the chromosomes organized during the interphase of the cell cycle, and how does the chromatin packing and chromosome positioning influence biological processes?

The organization of chromatin during the interphase can be analyzed by two methodological approaches: by high-throughput chromosome conformation capture (Hi-C) technique, followed by polymer modeling (Lieberman-Aiden *et al*., 2009; Giorgetti *et al.*, 2014; Gibcus *et al*., 2018), and by three-dimensional fluorescence in situ hybridization (3D-FISH) and microscopic techniques (Bass *et al.*, 1997). The Hi-C method combines 3C technique (Dekker *et al.*, 2002) and next-generation sequencing (Lieberman-Aiden *et al.*, 2009) to find out chromatin compaction. Recently, Hi-C techniques have been used in many living organisms to describe chromosome contact patterns, genome packing, and 3D chromatin architecture at much higher resolution (tens to hundreds of kilobases) than is

provided by 3D-FISH (Dong *et al.*, 2018; Dumur *et al.*, 2019; Concia *et al.*, 2020; Golicz *et al.*, 2020). On the other hand, majority of Hi-C studies in plant species were performed on pooled tissues and thus could not provide information about the variability in spatial organization of individual chromosomes in 3D space of the interphase nuclei (Wang *et al.*, 2015; Dong *et al.*, 2017; Concia *et al*., 2020). This information can be achieved by application of recently developed cytogenetic techniques, oligo-painting, and 3D-FISH, which enable to visualize individual genome regions in 3D space of nuclei (Howe *et al.*, 2013; Han *et al.*, 2015).

Hi-C studies in metazoans and mammals revealed the existence of megabase-long chromatin compartments containing either active and open chromatin (A compartments), or inactive and closed chromatin (B compartments). Hi-C also allowed to describe organization into smaller (in average 800 kb long in mammals), self-interacting topologically associated domains (TADs), regulatory landscapes of chromosomes, which were revealed in animal interphase nuclei (e.g. Sexton and Cavalli, 2015; Ramírez *et al*., 2018; Szabo *et al.*, 2018). Genes belonging to the same TADs display similar expression dynamics suggesting that their physical association is functionally related to gene expression control (de Graaf et al., 2013). In plants, 3D chromatin architecture is different. For instance, TADs were not observed in *A. thaliana* (Feng *et al*., 2014; Wang *et al*., 2015; Liu *et al*., 2017), instead their presence seems to be linked to species with larger genomes (Dong *et al.*, 2017; Liu *et al*., 2017; Concia *et al*., 2020; Golicz *et al*., 2020). Since TADs have not been recognized in all plant species, the question arises whether they play an important role in the dynamics of plant chromosomes.

Complementary cytogenetic data to Hi-C studies are still missing. In plant research, chromosome distribution in interphase nuclei was studied by FISH with probes specific to functional chromosome domains such as centromeres and telomeres (Hou *et al.*, 2018; Liu *et al.*, 2020). The aim of these studies was to confirm the first microscopic observations *done by* Carl Rabl, who predicted that chromosome positioning in interphase nuclei follows their orientation in the preceding mitosis (Rabl, 1885; reviewed by Cremer *et al.*, 2006). The so-called Rabl configuration, with centromeres and telomeres oriented on opposite poles of nuclei, was originally assigned to plants with large genomes (wheat, rye, barley) (Cremer *et al.*, 2001). The concept of a Rabl-like pattern in plant species with large genomes and non-Rabl organization of interphase chromosomes in plants with small and medium genomes has been disproved early after it was proposed (Fujimoto *et al.*, 2005). In rice, the majority of nuclei in somatic cells lack Rabl configuration (Prieto *et al.*, 2004; Santos and Show, 2004; Němečková *et al*., 2020), however, chromosomes of pre-meiotic cells in anthers or xylem-

vessel precursor cells seem to assume the Rabl configuration (Prieto *et al.*, 2004; Santos and Show, 2004). Compared to numerous studies on the centromere-telomere organization in plant interphase nuclei (Fujimoto *et al.*, 2005; Idziak *et al*., 2015; Nemečková *et al.*, 2020; Shan *et al*., 2021), the visualization of the spatial positioning of individual chromosomes during interphase stays widely unknown. The mutual position of chromosomes during interphase was studied in *Arabidopsis thaliana* using BAC pools-based chromosome painting technique, showing that individual chromosomes tend to occupy separated territories (Pečinka *et al.*, 2004). The extremely small genome of Arabidopsis is characterized by a specific, rosette-like, chromosome configuration (Armstrong *et al.*,2001; Fransz *et al.*, 2002), which was not observed in any other plant species, thus we can not expect that the chromosome organization and dynamics revealed in *Arabidopsis* is universal to other plant species. Robaszkiewicz *et al.* (2016) later analyzed chromosome positioning in the 3D space of *Brachypodium distachyon*, which possesses Rabl orientation, and provided the first insight into the large variability of the interphase chromosome organization. However, the high level of variability in mutual chromosome organization shown in the study, could have been caused by the use of nuclei isolated from the pooled root tissue (Robaszkiewicz *et al*., 2016).

Our present study provides the first insight into chromatin compaction and variability of the spatial organization of CTs during the interphase of the cell cycle in highly dynamic root meristematic cells and diversified leaf nuclei. The use of super-resolution STED microscopy revealed different levels of chromatin compaction in root and leaf nuclei. 3D immuno-FISH experiments with chromosome-specific painting probes showed different types of mutual CTs positioning which varied between the root and leaf interphase nuclei.

Key words

3D Immuno-FISH, chromosome painting, chromosome territory, rice, spatial organization, microscopy

Abbreviations

3D – three-dimensional

CenH3 – centromere-specific variant of histone H3

CT – chromosome territory

FISH – fluorescence *in situ* hybridization

HiC – high-throughput chromosome conformation capture
NOR – nucleolar organizer region
PAA – polyacrylamide
rDNA – ribosomal deoxyribonucleic acid
ROI – region of interest
RT – room temperature
STED – stimulated emission depletion
TADs – topologically associated domains

Material and methods

Plant material, seeds germination and sample preparation

Seeds of rice (*Oryza sativa*) cultivar Nipponbare (2n=2x=24) were obtained from Prof. Ohmido Nobuko, Kobe University, Japan. Seeds were soaked in distilled water and bubbled for 24 h. After that, seeds germinated in a biological incubator at 24°C in a glass Petri dish on moistened filter paper until the primary roots were 3-4 cm long. Suspension of intact nuclei was prepared according to Doležel *et al.* (1992). Briefly, root tips were cut and fixed with 2% (v/v) formaldehyde in Tris buffer (10 mM Tris, 10 mM Na2EDTA, 100 mM NaCl, 0.1% Triton X-100, 2 % formaldehyde, pH 7.5) at 4°C for 30 min and washed three times with Tris buffer at 4°C. Meristematic parts of root tips (~1 mm long) were excised from 70 roots per sample. Root meristems were homogenized in 500 µl LB01 buffer (Doležel *et al*., 1989) by Polytron PT 1200 homogenizer (Kinematica AG, Littua, Switzerland) for 13 s at 14 500 rpm. Finally, the suspensions were filtered through a 20 µm nylon mesh and analyzed using a FASCAria II SORP flow cytometer and sorter (BD Bioscience, San Jose, USA). Nuclei representing the G1 phase of the cell cycle were sorted into 1x meiocyte buffer (Bass *et al.*, 1997; Howe *et al.*, 2013).

Root microtome sectioning and FISH

Roots fixed with 2% (v/v) formaldehyde in Tris were embedded in Cryo-Gel (Leica Biosystems, ID:39475237) and cut onto a cryostat (Leica CM1950) at a thickness of 20 µm. The resulting segments were transferred to super-frost slide (Thermo Scientific). Slides were allowed to dry overnight at room temperature and then either immediately utilized for FISH or stored at 4 °C until use. Prior to FISH, slides with root segments in cryo-gel were washed for 10 min in 1x PBS and subsequently dehydrated in ethanol series (70%, 85%, 100%

ethanol), each for 2 min. Hybridization mix (50 µl) containing 50% (v/v) formamide, 10% (w/v) dextran sulfate in 2x SSC, 1 µg sheared salmon sperm DNA (Invitrogen, AM9680) and 200 ng per probe was added onto the slides and denatured for 8 min at 78°C and cooled slowly (50 °C 1 min, 45 °C 1 min, 40 °C 1 min, 38 °C 5 min). After that, slides were hybridized overnight at 37 °C. The next day, slides were washed 3x5 min in 4xSSC, and root sections were counterstained with DAPI in VECTASHIELD Antifade Mounting Medium (Vector Laboratories, Burlingame, CA, USA).

Probes for FISH

Oligonucleotides specific for individual chromosomes were identified in the reference genome sequence of *Oryza sativa* cv. Nipponbare (version_7.0; http://rice.uga.edu/; Kawahara et al., 2013) using the Chorus v2 program pipeline (Zhang *et al.*, 2021). Two sets of oligomers were synthesized by Arbor Biosciences (Ann Arbor, Michigan, USA). Labeled oligomer probes were prepared according to Han *et al.* (2015). Probes specific for the long and short arms of chromosome 2 were labeled by biotin-16-dUTP and by aminoallyl-dUTP-CY3, and chromosome 9 was labeled by digoxigenin-11-dUPT and aminoallyl-dUTP-CY5 (Jena Biosciences, Jena, Germany). The painting probe of longer chromosome 2 contained 40,000 unique 45-mers and the painting probe specific to short chromosome 9 contained 20,000 unique 45-mers. Probes specific for 45S ribosomal DNA were amplified using specific primers (Ohmido and Fukui, 1995) and directly labeled with aminoallyl-dUTP-CY5 (Jena Biosciences, Jena, Germany).

Immuno-staining and fluorescence in situ hybridization (FISH)

Flow sorted nuclei were mounted in polyacrylamide gel according to Němečková *et al.* (2020). To visualize 45S rDNA, chromosome 2 and chromosome 9 together with fibrillarin, staining procedures, and washes were performed according to Němečková *et al.* (2020). Primary antibody anti-fibrillarin was diluted at 1:100 (ab4566, Abcam, Cambridge, UK). The hybridization mix for FISH contained 400 ng of individual probes.

Spirochrome staining and sample preparation for STED

Flow sorted nuclei were mounted in polyacrylamide gel onto silane-cover glass. High-precision cover glasses were prepared according to de Almeida Engler (2001) with modifications. Slides were washed in water for 15 min and in ethanol for 30 min. Slides were air dried for 10 minutes and then freshly prepared 2% 3-aminopropyltriethoxysilane (Sigma)

in acetone was applied for 30 min. Slides were washed twice in distilled water, dried overnight at 37°C, and stored at room temperature (RT). After gel polymerization, polyacrylamide pads were washed in MBA buffer (Howe *et al.*, 2013; Bass *et al*., 2014) and let dry at RT. Next, glycerol mounting medium AD-MOUNT S (ADVi, Říčany, Czech Republic) with SPY650-DNA (diluted 1:1000) (Spirochrome AG, cat#: SC501, Stein am Rhein, Switzerland) was applied onto the pads and covered with a microscopic slide.

Confocal and STED microscopy, and image analysis

Images were acquired using Leica TCS SP8 STED 3X confocal microscope (Leica Microsystems, Wetzlar, Germany) equipped with 63x/1.4 NA Oil Plan Apochromat objective and Leica LAS-X software with Leica Lightning module. Image stacks were captured separately for each chromosome using 647 nm, 561 nm, 488, and 405 nm laser lines for excitation and appropriate emission filters. Typically, an image stack of about 50 slides with 0.15 µm spacing was acquired. Root sections were acquired via the Navigator module using a 63x objective and the final picture was created by the mosaic merge function. Different chromatin structure of leaf and root was captured in the STED mode with *100x 1.4 NA STED oil objective*. The pinhole was set to 0.75 AU. The resolution was estimated using LAS-X software according to full width at half maximum criterion. The chromatin signal labeled by spirochrom (SPY650-DNA) was captured with a lateral resolution of c. 52 nm. LAS-X software was also used to produce color heat maps of individual nuclei.

3D models of microscopic images and volume calculations were performed using Imaris 9.7 software (Bitplane, Oxford Instruments, Zurich, Switzerland). The volume of each nucleus, nucleolus, and chromosome territories was estimated based on the primary intensity of fluorescence obtained by microscopy. Imaris function ‘Surface’ was used for modeling the chromosome arrangement in the nucleus and for modeling the 45S rDNA, chromosomes, and fibrillarin. Chanel contrast was adjusted using ‘Chanel Adjustment’ and videos were created using the ‘Animation function’. About 100 nuclei were analyzed for each selected variant.

Results

Variation in chromatin condensation and nuclei features

To analyze and compare the level of chromatin condensation in G1 interphase nuclei of young leaves and root meristems, we applied stimulated emission depletion (STED) microscopy. With this aim, mildly fixed flow sorted G1 nuclei from leaves and root

meristems were mounted in polyacrylamide gel onto silane-coated high-precision cover glass to ensure their 3D structure will be preserved. STED analysis uncovered detailed chromatin ultrastructure and revealed differences in the level of chromatin compaction between G1 nuclei isolated from leaves and root meristems. G1 nuclei of root meristem, which undergo repeated and rapid cell division, were characterized by more relaxed chromatin and apparent ultra-structures (Figure 1A). In comparison, a more compact structure of chromatin and presence of lower amount of interchromatin compartments was found in G1 nuclei isolated from differentiated leaf cells (Figure 1A). The chromatin condensation in G1 nuclei isolated from both tissues were also visualized as color heat maps (e.g. Cremer *et al.*, 2017; Cremer and Cremer, 2019), which display differences in the general chromatin organization between root meristem and leaf G1 nuclei (Figure 1A). The width of chromatin fiber in G1 nuclei from leaf reached 240 nm on average, while in root, the chromatin fiber was three times narrower, about 83 nm in width (Figure 1B)

Likewise, the nuclei volume of G1 nuclei isolated from root meristematic zones was more than three times higher (199 µm3) compared to leaf nuclei (59.6 µm3) (Table 1). Similarly, volumes of nucleoli, which were visualized by immunodetection with nucleolus-specific protein fibrillarin, varied between leaves and root meristem. The volume of root nucleoli occupied 14.13 µm3 on average, which represents 7.1 % of the volume of the root nucleus (Supplementary video 1). Leaf nucleolus occupied 0.7 µm3, representing only 1.2 % of the leaf nucleus. (Table 1; Supplementary video 2).

Further analyses of about 200 G1 nuclei specific for both analyzed tissues revealed also variation in their shapes (Figure 2A). Majority of the nuclei had elliptical shape (~ 67 %), and the rest of the G1 nuclei had spindle-like (~ 21 %) and donut-like (~ 13 %) shapes in root meristematic cells. Proportion of the G1 nuclei shapes was almost identical for both studied tissues (Table 1, Figure 2A).

Chromosome specific painting probes

With the aim to analyze positioning of whole chromosomes during the interphase, we prepared oligo-painting probes for two rice chromosomes. Based on the previous Hi-C results, which proposed presence of two sets of chromosomes differing in level of their association (Dong *et al.*, 2018), we analyzed detailed positioning of two chromosomes representing the two different sets. Long, sub-metacentric chromosome 2 (member of chromosome set which showed close association), and short acrocentric chromosome 9 containing NOR region and belonging to the set of chromosomes which did not show apparent association (Dong *et al.*,

2018). Painting probes specific for both chromosomes were designed from a set of non-overlapping unique oligomers identified in reference genome sequence of *Oryza sativa* cv. Nipponbare v.7.0 (Kawahara *et al.*, 2013) using Chorus v2 program pipeline (Zhang *et al.*, 2021). Both oligos libraries were designed to achieve a density of at least 0.9 oligo per kb to ensure good visibility of hybridization signals after FISH. Sensitivity and suitability of the painting probe for chromosome identification *in situ* was confirmed by FISH on prometaphase and metaphase chromosomes (Figure 2C, 2D), and further on flow sorted G1 nuclei of root (Figure 3A, 3C, 3D) meristem and leaf tissue (Figure 3B). Both probes produced bright signals without any cross-hybridization. As expected, painting probes were strongly localized to chromosome arms, and centromeric regions and NOR region (containing specific repetitive DNA sequences) remained without good visible signal (Figure 2C, 2D).

Mutual position of chromosomes in G1 interphase nuclei

3D-FISH with the chromosome painting probes on G1 nuclei of rice revealed presence of compact structures in both examined tissue types and confirmed presence of so-called chromosome territories (CTs), which were predicted by Hi-C studies (Dong *et al.*, 2018). Painting FISH revealed variability in constitution of the CTs, which were present either as two separated territories corresponding to two homologous chromosomes in G1 nuclei (Figure 2E, 3A, 3C), or as one large territory in which homologous chromosomes were tightly connected (Figure 3B). In general, higher proportion of G1 nuclei isolated from leave tissue showed close association of homologous chromosomes which were visualized as one large CT (63 % for chromosome 9; and 59 % for chromosome 2) compared to root meristem, which mostly contained G1 nuclei with two separated CTs (87 % for chromosome 9; and 59 % for chromosome 2) (Figure 4).

Comparison of both territory volumes corresponding to homologous chromosomes did not reveal significant differences. Both chromosome territories represented 8.2 % of nucleus volume in root meristematic cells and 8.8% of the nucleus of leaf cells. The volume of separated territories of chromosome 2 was estimated to occupy approximately 4 % of the nucleus volume in both plant tissues (Table 2).

Co-hybridization and visualization of both chromosomes showed six different types of their mutual arrangement in G1 nuclei of root meristem (Figure 4A). About 45,3 % of examined root meristematic nuclei contained chromosomes 2 and 9 organized in two separate CTs concurrently, and additional 27,4 % of the nuclei contained chromosome 9 arranged in two separate CTs, and chromosome 2 in one large CT. 14,7 % of analyzed nuclei contained

two nucleoli and in all these cases, CTs of chromosome 9 were separated. (Figure 4A).

In comparison, only four different arrangements of chromosome 2 and 9 were observed in leaf G1 nuclei. Nuclei containing two nucleoli were not present. 36.7 % of leaf nuclei contained two large CTs corresponding to chromosomes 2 and 9, other nuclei contained one large CT of chromosome 9 and two separated CTs specific to chromosome 2 (26.4 %). In the similar number of nuclei (22.2 %) CTs of homologous chromosome 2 were associated, and CTs of chromosome 9 were separated. Finally, 14.4 % of leaf G1 nuclei contained both chromosomes arranged in separate CTs (Figure 4A).

The difference in the proportion of separated and associated CTs between chromosomes 2 and 9 can be caused by the presence of NOR region on the short arm of chromosome 9. NOR region consists of 45S rRNA genes which constitute nucleoli, so the position of chromosome 9 in interphase nuclei also depends on the position and nature of the nucleolus/nucleoli (Supplementary Figure 1). A detailed 3D analysis revealed different numbers of 45S rDNA loci in the root and leaf. In the root, two major loci were usually observed on the periphery of the nucleolus and 2-4 small signals were observed inside the nucleolus (Supplementary Figure 1, Table 3). In comparison, only 1-2 45S rDNA loci situated on the periphery of the nucleolus were observed in the leaf, where the nucleolus occupies much lower volume (Supplementary Figure 1, Table 3).

Detailed image analysis of leaf G1 nuclei revealed that the position of chromosome 2 is more random compared to chromosome 9. Large sub-metacentric chromosome 2 was in most cases arranged through the entire nucleus volume in the z-axis, with a large region located on the nuclear periphery (Figure 5). Even though, chromosome 2 does not contain rRNA genes and is not directly connected to nucleoli, its spatial positioning seems to be influenced by the nature of nucleoli (size, number, and position inside the nucleus).

As we mentioned above, the G1 nuclei of both tissues varied also in their shape (Table 1, Figure 2A), thus we investigated relations between the CTs arrangement and nuclei shapes. Our data showed, that specific arrangements of CTs did not correlate with different shapes of nuclei. Despite lower proportion of spindle and donut-like nuclei (Table 1, Figure 2B), all CTs rearrangements (two separated territories, and homologous chromosome associated territory specific to chromosomes 2 and 9) were present in all examined nuclei (Figure 2B). Nevertheless, the potential connection between dominant pattern of CTs and the nuclear shape needs to be investigated in more detail on larger sample set due to unequal representation of spindle and donut-like nuclei (Table 1, Figure 2B).

Finally, we investigated the patterns of chromosome positioning in different cell types

of the root meristem tissue. As we showed earlier, rice root meristematic cells did not show Rabl configuration of chromosomes during the interphase of the cell cycle (Němečková *et al.*, 2020). The only exception was described by Prieto *et al.* (2004). They showed that xylem vessel cells, which are bigger and probably containing endoreduplicated nuclei, tend to achieve Rabl configuration. To confirm these findings by 3D FISH, we localized probes specific to centromeric and telomeric sequences on ultra-thin root sections prepared by cryomicrotome. Rabl configuration was observed in rice xylem vessel cells as well as in cortex cells (Figure 6A, B). Both cell types are bigger and the volume measurements of their nuclei performed in Imaris software indicate the presence of the endoreduplication. Unfortunately, proportion of these specific cell types in roots of rice is very low, so it is not possible to identify them by flow cytometry, estimate their DNA content and thus confirm presence of endoreduplication.

Disscusion

Early studies of chromatin structure which used electron microscopy suggested its helical arrangement into 30 nm nucleosome fiber (Finch and Klug, 1976; Woodcock *et al.*, 1984; Bordas *et al.*, 1986). However, this model of chromatin folding and its higher-order organization became controversial due to the difference in observation between in vivo and in vitro conditions (Maeshima *et al.*, 2019; Prieto et Maeshima, 2019). Recent development of super-resolution microscopy techniques, which enable to reach a resolution of about 1-250 nm (reviewed in Valli *et al.*, 2021), allowed to describe a presence of 100-200 nm higher-order chromonema fibers (Kireeva *et al.*, 2004; Maison *et al.*, 2010; Belmont, 2014). Studies of DNA replication foci in human cells proposed a globular folding of chromatin with a diameter of about 110-150 nm (Jackson and Pombo, 1998; Albiez *et al.*, 2006; Cseresnyes *et al.*, 2009; Markaki *et al.*, 2012).

In our study, we have analyzed chromatin compaction in the interphase nuclei of highly dynamic root meristematic cells and nuclei isolated from differentiated leaf cells. We have used STED super-resolution microscopy which can reach xy-resolution less than 60 nm, and also enables acquisition of three-dimensional images (Dumur *et al.*, 2019; Moors *et al.*, 2021; Frolikova *et al.*, 2023). To provide information on chromatin compaction during the interphase of the cell cycle, mild formaldehyde fixation of the nuclei and their further mounting in polyacrylamide gel was used to preserve 3D chromatin structure and to avoid chromatin destruction during sample preparation (Bass *et al.*, 2014; Howe *et al.*, 2013; Němečková *et al.*, 2020). Another important feature of the sample preparation for STED

375 microscopy was the selection of appropriate mounting media, which would not have negative
376 effect on 3D structure of the nuclei (Koláčková *et al.*, in preparation).
377 Striking difference in chromatin compaction in G1 nuclei of root and leaf tissues were
378 observed (Figure 1). Presence of 80 nm chromatin fibers was revealed in rice root
379 meristematic G1 nuclei. Similar width of chromatin fiber (70 nm) was observed in metaphase
380 chromosomes of Drosophila (Matsuda *et al.*, 2010) and recently in mitotic chromosomes of
381 barley root meristem (Kubalová *et al*., 2023). These results could indicate that the higher level
382 of chromatin spiralization, which is typical for mitotic chromosomes, is maintained in
383 interphase nuclei of highly dynamic meristematic cells. On the contrary, the diameter of rice
384 leaf chromatin fibers was three times higher, reaching 240 nm. Similar variability in
385 chromatin fibers was observed in human and animal studies, including metazoans (reviewed
386 by Hansen et al., 2018). Actually, studies of Belmont *et al.* (1994) and Dehghani *et al.* (2005)
387 showed presence of two classes of chromatin fibers, with diameters 60-80 nm, and 100-130
388 nm in early G1 and late G1/early S. Described diameter of rice higher order chromatin
389 structure correlates with the diameter of the He-la cells' higher-order chromatin structure (220
390 nm) (Nozaki *et al.*, 2017). Root meristem and leaf nuclei varied also in the volume and level
391 of chromatin compactness. Root meristem G1 nuclei were more than three times larger and
392 consist of more relaxed chromatin with higher proportion of interchromatin compartments
393 (Figure 1). As we analyzed G1 nuclei of highly dynamic root meristem cells, we can
394 speculate, that the bigger size of these nuclei and higher proportion of interchromatin
395 compartments are needed for the synthesis of mRNA and proteins, which are required for
396 DNA synthesis in the following S phase. In comparison, differentiated cells of leaf tissues
397 contained smaller G1 nuclei consisting of more compact chromatin with lower proportion of
398 interchromatin compartments, where transcription takes a place, as was demonstrated in
399 human studies (Hübner *et al.*, 2015; Cremer et Cremer, 2019).
400 Recently, it was shown that nuclear architecture, the size and shape, and positioning of CTs
401 during interphase, can be influenced by several factors, especially the size of a given
402 chromosome, position of centromere, and the shape of nucleolus. In *Brachypodium*
403 *distachyon*, a plant species that maintains Rabl configuration, a high level of homologous CTs
404 associations was found in spherical nuclei, while it was negatively correlated with elongated
405 nuclei (Robaszikewicz *et al*., 2016). Similar results were described for plants with rosette-like
406 chromosome conformation in the nuclei of both, root and leaf, tissues (Pečinka *et al*., 2004).
407 In our study, mutual position of two morphologically different chromosomes in interphase
408 nuclei was not correlated with the nuclei shape. On the other hand, we revealed differences in

organization and mutual chromosome position between root meristem and leaf G1 nuclei. We observed presence of discrete chromosome territories specific to both visualized chromosomes. CTs of NOR bearing chromosome 9 were mostly separated in root meristem nuclei, while their (CTs) association prevailed in leaf G1 nuclei, regardless their shape. Our findings are not in agreement with the organization and distribution of CTs of NOR bearing chromosome in *Brachypodium*, which were predominantly associated (59,3 %) (Robaszkiewicz *et al.*, 2016). Robaszkiewicz *et al.* (2016) also suggested, that the length of a particular chromosome may influence the dominant pattern of its spatial arrangement inside the nucleus, and showed that CTs of the longest chromosome were usually associated. However, the high level of variability in mutual chromosome organization shown in the study of Robaszkiewicz *et al.* (2016) could be caused by the analysis of nuclei isolated from the pooled root tissue. Random positioning of most CTs was observed in *Arabidopsis*. The only exception was the position of NOR bearing chromosomes, which seemed to be connected to the position of nucleoli (Lysak *et al.*, 2001; Pecinka *et al.*, 2004; Berr and Schubert, 2007).

Spatial organization and mutual position of CTs in 3D space of large plant genomes with Rabl configuration have not yet been analyzed by in situ techniques. The only exception was the visualization of alien chromosomes in wheat-rye and wheat-barley introgression lines (Koláčková *et al.*, 2019; Perníčková *et al.*, 2019). In both cases, a complete separation of CTs corresponding to alien chromosomes was observed in majority (83 – 89 %) of studied root meristem cells (Koláčková *et al.*, 2019; Perníčková *et al.*, 2019).

The discrepancies in CTs organization and positioning in 3D nuclear space between our work and previous studies, especially those of Robaszkiewicz *et al.* (2016), could be also caused by the difference of chromosome configuration (Rabl and non-Rabl) in the studied species. Further investigation has to be done to find out if chromosome configuration affects the organization and mutual position of CTs during the interphase of the cell cycle.

As we already mentioned, the shape and number of nucleoli represent another factor, which can affect the CTs positioning. Derenzini *et al.* (1998) showed, that cancer dividing cells produced elevated amounts of rRNA and often possessed large nucleoli whereas down-regulation of rRNA gene transcription led to reduction in nucleolar size. More recently, Tiku *et al.* (2018) showed, that size of the nucleolus positively correlates with rRNA synthesis. Analysis of purified nucleoli of *A. thaliana* showed that active rRNA genes are present within nucleoli whereas silent copies are excluded (Pontviane *et al.*, 2013). Correlation between rRNA activity and arrangement of chromosome territories was indicated also in our study. Homologs of chromosome 9 were organized into separated territories (in 93 % of all events)

in G1 nuclei of root meristem, where the rRNA genes are being highly expressed (Tulpová *et al.*, 2022). On the other hand, chromosome 9 was more associated (59 % associated, 41 % separated) in leaf tissue, in which smaller volume of nucleolus and only 1-2 clusters of 45s rDNA were observed.

Our study showed high rate of variability in mutual chromosome positioning in the 3D space of G1 nuclei isolated from both plant tissues. This variability in the association/separation of homologous CTs may reflect the interphase chromatin dynamics. Movement of chromatin was described in *Arabidopsis* interphase nuclei by visualization of tagged loci in live seedlings (Kato and Lam, 2003), and in yeast (e.g. Heun, 2001; Bystricky *et al.*, 2004; Hajjoul *et al.*, 2013), animal and human cells (e.g. Chubb *et al.*, 2002; Levi *et al.*, 2005, Germier *et al.*, 2017; Nozaki *et al.*, 2023).

The observed heterogeneity in chromosome positioning and variability in chromatin condensation within different tissues explain the discrepancy between contact frequencies and distance distributions obtained by Hi-C and 3D-FISH (Fudenberg *et al.*, 2017). In plants, most Hi-C studies, which can be also used to create putative models of chromatin condensation and chromosome positioning, were done on pooled tissues (Wang *et al.*, 2015; Dong *et al.*, 2017; Concia *et al.*, 2020). Therefore, 3D modeling was performed based on averages of large numbers of cells, and the information on potential variability in 3D structure among different cells or cell types was lost. This can be overcome by single-cell Hi-C (scHi-C) experiments (Nagano *et al.*, 2013; Ramani *et al.*, 2017; Tan *et al.*, 2018). In plant research, scHi-C experiments are not numerous. For instance, in rice, this technique was used to study variability in chromatin organization in eggs, sperm cells, unicellular zygotes, and shoot mesophyll cells. Even though the analysis was performed only on four cells representing each tissue type, theoretical models of chromosome folding and their mutual organization indicated variability in the positioning of chromosome territories among the analyzed nuclei (Zhou *et al.*, 2019).

To conclude our study, we showed that advanced microscopy combined with recent cytogenetics techniques is a powerful tool for analysis and comparison of mutual chromosomes positions in the nuclei during the interphase of the cell cycle. Our experiments support the hypothesis, that chromatin organization is not determined by the shape of the nucleus. On the other hand, it appears that the size of the nucleolus and its position in the nucleus plays a role in chromosome positioning during interphase. The analysis of large number of nuclei confirms variability in chromosome organization into nuclear territories and their mutual positioning within and also between nuclei isolated from different tissue types.

Furthermore, the use of super-resolution STED microscopy corroborates striking differences in chromatin folding and organization in the interphase nuclei isolated from the two studied plant tissues.

Acknowledgments

We would like to cordially thank Jitka Weiserová and Dr. Petr Cápal for flow sorting, Zdeňka Dubská for excellent technical assistance, and Lucie Kobrlová for enabling the sample preparation on cryomicrotome and for the technical support. We would like to thank Dr. Jana Čížková for her valuable comments. The computing was supported by the project "e-Infrastruktura CZ" (e-INFRA CZ LM2018140) supported by the Ministry of Education, Youth and Sports of the Czech Republic, and by the ELIXIR-CZ project (LM2018131), part of the international ELIXIR infrastructure. This research was funded by the ERDF project "Plants as a tool for sustainable global development" (No. CZ.02.1.01/0.0/0.0/16_019/0000827).

Author Contributions

E.H., and A.D. conceived the project. E.H. and D.B. designed and prepared painting probes, A.D., D.B., and V.K. conducted cytogenetic part of the work. A.D. and E.H., wrote the original draft, D.B. and V.K., reviewed and edited the manuscript. All authors have read and approved the final manuscript.

Conflicts of Interest

The authors declare no conflicts of interest.

Literature

Albiez H, Creme, M, Tiberi C, Vecchio L, Schermelleh L, Dittrich S, Küpper K, Joffe B, Thormeyer T, von Hase J, Yang S, Rohr K, Leonhardt H, Solovei I, Cremer C, Fakan S, Cremer T. 2006. Chromatin domains and the interchromatin compartment form structurally defined and functionally interacting nuclear networks. *Chromosome Res* 14, 707–733. https://doi.org/10.1007/s10577-006-1086-x

511 Armstrong SJ, Franklin FCH, Jones GH. 2001. Nucleolus-associated telomere clustering and
512 pairing precede meiotic chromosome synapsis in *Arabidopsis thaliana*. *Journal of Cell*
513 *Science* 114(23), 4207-4217. https://doi.org/10.1242/jcs.114.23.4207

514 Bass HW, Marshall WF, Sedat JW, Agard DA, Cande WZ. 1997. Telomeres cluster de novo
515 before the initiation of synapsis: a three-dimensional spatial analysis of telomere positions
516 before and during meiotic prophase. *The Journal of cell biology* 137(1), 5-18.
517 https://doi.org/10.1083/jcb.137.1.5

518 Bass HW, Wear EE, Lee TJ, Hoffman GG, Gumber HK, Allen GC, Thompson WF, Hanley-
519 Bowdoin L. 2014. A maize root tip system to study DNA replication programmes in somatic
520 and endocycling nuclei during plant development. *Journal of experimental botany* 65, 2747-
521 2756. https://doi.org/10.1093/jxb/ert470

522 Belmont AS. 2014. Large-scale chromatin organization: the good, the surprising, and the still
523 perplexing. *Current opinion in cell biology* 26, 69-78.
524 https://doi.org/10.1016/j.ceb.2013.10.002

525 Belmont AS and Bruce K. 1994. Visualization of G1 chromosomes: a folded, twisted,
526 supercoiled chromonema model of interphase chromatid structure. *The Journal of cell*
527 *biology* 127(2), 287-302. https://doi.org/10.1083/jcb.127.2.287

528 Berr A and Schubert I. 2007. Interphase chromosome arrangement in *Arabidopsis thaliana* is
529 similar in differentiated and meristematic tissues and shows a transient mirror symmetry after
530 nuclear division. *Genetics* 176, 853–863. https://doi.org/10.1534/genetics.107.073270

531 Bordas J, Perez-Grau L, Koch MHJ, Vega MC, Nave C. 1986. The superstructure of
532 chromatin and its condensation mechanism: II. Theoretical analysis of the x-ray scattering
533 patterns and model calculations. *European Biophysics Journal* 13, 175-185.
534 https://doi.org/10.1007/BF00542561

535 Bystricky K, Heun P, Gehlen L, Langowski J, Gasser SM. 2004. Long range compaction and
536 flexibility of interphase chromatin in budding yeast analysed by high-resolution imaging
537 techniques. *Proceedings of the National Academy of Sciences* 101: 16495–16500.
538 https://doi.org/10.1073/pnas.0402766101

539 Chubb JR, Boyle S, Perry P, Bickmore WA. 2002. Chromatin motion is constrained by
540 association with nuclear compartments in human cells. *Current Biology* 12(6), 439-445.
541 https://doi.org/10.1016/S0960-9822(02)00695-4

542 Concia L, Veluchamy A, Ramirez-Prado JS, Martin-Ramirez A, Huang Y, Perez M,
543 Domenichini S, Rodriguez Granados NY, Kim S, Blein T, Duncan S, Pichot C, Manza-
544 Mianza D, Juery C, Paux E, Moore G, Hirt H, Bergounioux C, Crespi M, Mahfouz MM,
545 Bendahmane A, Liu C, Hall A, Raynaud C, Latrasse D, Benhamed M.. 2020. Wheat
546 chromatin architecture is organized in genome territories and transcription factories. *Genome*
547 *Biology* 21, 1-20. https://doi.org/10.1186/s13059-020-01998-1

548 Cremer M and Cremer T. 2019. Nuclear compartmentalization, dynamics, and function of
549 regulatory DNA sequences. *Genes, Chromosomes and Cancer* 58(7), 427-436.
550 https://doi.org/10.1002/gcc.22714

551 Cremer M, Schmid VJ, Kraus F, Markaki Y, Hellmann I, Maiser A, Leonhardt H, John S,
552 Stamatoyannopoulos J, Cremer T. 2017. Initial high-resolution microscopic mapping of active
553 and inactive regulatory sequences proves non-random 3D arrangements in chromatin domain
554 clusters. *Epigenetics & chromatin* 10, 1-17. https://doi.org/10.1186/s13072-017-0146-0

555 Cremer M, von Hase J, Volm T, Brero A, Kreth G, Walter J, Fischer C, Solovei I, Cremer C,
556 Cremer T. 2001 Non-random radial higher-order chromatin arrangements in nuclei of diploid
557 human cells. *Chromosome Research* 9, 541–567. https://doi.org/10.1023/A:1012495201697

558 Cremer T, Cremer M, Dietzel S, Müller S, Solovei I, Fakan S. 2006. Chromosome territories–
559 a functional nuclear landscape. C*urrent Opinion in Cell Biology* 18(3), 307-316.
560 https://doi.org/10.1016/j.ceb.2006.04.007

561 Cseresnyes Z, Schwarz U, Green CM. 2009 Analysis of replication factories in human cells
562 by super-resolution light microscopy. *BMC Cell Biology* 10, 88. https://doi.org/10.1186/1471-
563 2121-10-88

564 de Almeida Engler J, De Groodt R, Van Montagu M, Engler G. 2001. *In situ* hybridization to
565 mRNA of *Arabidopsis* tissue sections. *Methods* 23(4), 325-334.
566 https://doi.org/10.1006/meth.2000.1144.

567 de Graaf CA and van Steensel B. 2013. Chromatin organization: form to function. *Current*
568 *Opinion in Genetics & Development* 23(2), 185-190.
569 https://doi.org/10.1016/j.gde.2012.11.011

570 Dehghani H, Dellaire G, Bazett-Jones DP. 2005. Organization of chromatin in the interphase
571 mammalian cell. *Micron* 36(2), 95-108. https://doi.org/10.1016/j.micron.2004.10.003

572 Dekker J, Rippe K, Dekker M, Kleckner N. 2002. Capturing chromosome

573 conformation. *Science* 295(5558), 1306-1311. https://doi.org/10.1126/science.1067799

574 Derenzini M, Trere D, Pession A, Montanaro L, Sirri V, Ochs RL. 1998. Nucleolar function
575 and size in cancer cells. *The American Journal of Pathology* 152(5), 1291.

576 Doležel J, Binarová P, Lucretti S. 1989. Analysis of nuclear DNA content in plant cells by
577 flow cytometry. *Biologia Plantarum* 31, 113–120.

578 Doležel J, Sgorbati S, Lucretti S. 1992. Comparison of three DNA fluorochromes for flow
579 cytometric estimation of nuclear DNA content in plants. *Physiologia Plantarum* 85, 625-631.

580 Dong P, Tu X, Chu PY, Lü P, Zhu N, Grierson D, Du B, Li P, Zhong S. 2017. 3D chromatin
581 architecture of large plant genomes determined by local A/B compartments. *Molecular Plant*
582 10(12), 1497-1509. https://doi.org/10.1016/j.molp.2017.11.005

583 Dong Q, Li N, Li X,Yuan Z, Xie D, Wang X, Li J, Yu Y, Wang J, Ding B, Zhang Z, Li C,
584 Bian Y, Zhang A, Wu Y, Liu B, Gong L. 2018. Genome-wide Hi-C analysis reveals extensive
585 hierarchical chromatin interactions in rice. *The Plant Journal* 94(6), 1141-1156.
586 https://doi.org/10.1111/tpj.13925

587 Dumur T, Duncan S, Graumann K, Desset S, Randall RS, Scheid OM, Prodanov D, Tatout C,
588 Baroux C. 2019. Probing the 3D architecture of the plant nucleus with microscopy
589 approaches: challenges and solutions. *Nucleus* 10(1), 181-212.
590 https://doi.org/10.1080/19491034.2019.1644592

591 Feng S, Cokus SJ, Schubert V, Zhai J, Pellegrini M, Jacobsen SE. 2014. Genome-wide Hi-C
592 analyses in wild-type and mutants reveal high-resolution chromatin interactions in
593 *Arabidopsis*. *Molecular Cell* 55(5), 694-707. https://doi.org/10.1016/j.molcel.2014.07.008

594 Finch JT and Klug A. 1976. Solenoidal model for superstructure in chromatin. *Proceedings of*
595 *the National Academy of Sciences* 73(6), 1897-1901. https://doi.org/10.1073/pnas.73.6.1897

596 Fransz P, De Jong JH, Lysak M, Castiglione MR, Schubert I. 2002. Interphase chromosomes
597 in *Arabidopsis* are organized as well defined chromocenters from which euchromatin loops
598 emanate. *Proceedings of the National Academy of Sciences* 99(22), 14584-14589.
599 https://doi.org/10.1073/pnas.212325299

600 Frolikova M, Blazikova M, Capek M, Chmelova H, Valecka J, Kolackova V, Valaskova E,
601 Komrskova K, Horvath O, Novotny I. 2023. A sample preparation procedure enables
602 acquisition of 2-channel super-resolution 3D STED image of an entire oocyte. bioRxiv, 2023-
603 03. https://doi.org/10.1101/2023.03.07.531472

Fudenberg G and Imakaev M. 2017. FISH-ing for captured contacts: towards reconciling FISH and 3C. *Nature Methods* 14(7), 673-678. 10.1038/nmeth.4329

Fujimoto S, Ito M, Matsunaga S, Fukui K. 2005. An upper limit of the ratio of DNA volume to nuclear volume exists in plants. *Genes & Genetic System* 80, 345–350. https://doi.org/10.1266/ggs.80.345

Germier T, Kocanova S, Walther N, Bancaud A, Shaban HA, Sellou H, Politi AZ, Ellenberg J, Gallardo F, Bystricky K. 2017. Real-time imaging of a single gene reveals transcription-initiated local confinement. *Biophysical Journal* 113(7), 1383-1394. https://doi.org/10.1016/j.bpj.2017.08.014

Gibcus JH, Samejima K, Goloborodko A, Samejima I, Naumova N, Nuebler J, Dekker J. 2018. A pathway for mitotic chromosome formation. *Science* 359(6376), eaao6135. https://doi.org/10.1126/science.aao6135

Giorgetti L, Galupa R, Nora EP, Piolot T, Lam F, Dekker J, Tiana G, Heard E. 2014. Predictive polymer modeling reveals coupled fluctuations in chromosome conformation and transcription. *Cell* 157.4 (2014): 950-963. https://doi.org/10.1016/j.cell.2014.03.025

Golicz AA, Bhalla PL, Edwards D, Singh MB. 2020. Rice 3D chromatin structure correlates with sequence variation and meiotic recombination rate. *Communications Biology* 3(1), 235. https://doi.org/10.1038/s42003-020-0932-2

Hajjoul H, Mathon J, Ranchon H, Goiffon I, Mozziconaci J, Albert B, Carrivain P, Victor J-M, Gadal O, Bystricky K, Bancaud A. 2013. High-throughput chromatin motion tracking in living yeast reveals the flexibility of the fiber throughout the genome. *Genome Research* 23(11), 1829-1838. https://doi.org/10.1101/gr.157008.113

Han Y, Zhang T, Thammapichai P, Weng Y, Jiang J. 2015. Chromosome-specific painting in *Cucumis* species using bulked oligonucleotides. *Genetics* 200, 771–779. doi: 10.1534/genetics.115.177642. https://doi.org/10.1534/genetics.115.177642

Hansen JC, Connolly M, McDonald CJ, Pan A, Pryamkova A, Ray K, Seidel E, Tamura E, Rogge R, Maeshima K. 2018. The 10-nm chromatin fiber and its relationship to interphase chromosome organization. *Biochemical Society Transactions* 46(1), 67-76. https://doi.org/10.1042/BST20170101

Heun P, Laroche T, Shimada K, Furrer P, Gasser S. 2001. Chromosome dynamics in the yeast interphase nucleus. *Science* 294: 2181. https://doi.org/10.1126/science.1065366

635 Hou L, Xu M, Zhang T, Xu Z, Wang W, Zhang J, Yu M, Ji W, Zhu C, Gong Z, Gu M, Jiang
636 J, Yu H. 2018. Chromosome painting and its applications in cultivated and wild rice. *BMC*
637 *Plant Biology* 18(1), 1-10. https://doi.org/10.1186/s12870-018-1325-2

638 Howe ES, Murphy SP, Bass HW. 2013. Three-dimensional acrylamide fluorescence *in situ*
639 hybridization for plant cells. In Plant meiosis. Humana Press, Totowa, NJ, 53-66.
640 https://doi.org/10.1007/978-1-62703-333-6_6

641 Hübner B, Lomiento M, Mammoli F, Illner D, Markaki Y, Ferrari S, Cremer M, Cremer T.
642 2015. Remodeling of nuclear landscapes during human myelopoietic cell differentiation
643 maintains co-aligned active and inactive nuclear compartments. *Epigenetics & Chromatin* 8,
644 1-21. https://doi.org/10.1186/s13072-015-0038-0

645 Idziak D, Robaszkiewicz E, Hasterok R. 2015. Spatial distribution of centromeres and
646 telomeres at interphase varies among *Brachypodium* species. *Journal of Experimental*
647 *Botany* 66(21), 6623-6634. https://doi.org/10.1093/jxb/erv369

648 Jackson DA, Pombo A. 1998. Replicon clusters are stable units of chromosome structure:
649 evidence that nuclear organization contributes to the efficient activation and propagation of S
650 phase in human cells. *Jornal of Cell Biology* 140:1285–1295.
651 https://doi.org/10.1083/jcb.140.6.1285

652 Kato N and Lam E. 2003. Chromatin of endoreduplicated pavement cells has greater range of
653 movement than that of diploid guard cells in *Arabidopsis thaliana*. *Journal of Cell*
654 *Science* 116(11), 2195-2201. https://doi.org/10.1242/jcs.00437

655 Kawahara Y, de la Bastide M, Hamilton JP, Kanamori H, McCombie WR, Ouyang S,
656 Schwartz DC, Tanaka T, Wu J, Zhou S, Childs KL, Davidson RM, Lin H, Quesada-Ocampo
657 L, Vaillancourt B, Sakai H, Lee SS, Kim J, Numa H, Itoh T, Buell CR, Matsumoto T. 2013.
658 Improvement of the *Oryza sativa* Nipponbare reference genome using next generation
659 sequence and optical map data. *Rice* 6, 1-10. https://doi.org/10.1186/1939-8433-6-4

660 Kireeva N, Lakonishok M, Kireev I, Hirano T, Belmont AS. 2004. Visualization of early
661 chromosome condensation: a hierarchical folding, axial glue model of chromosome
662 structure. *Journal of Cell Biology* 166:775–785. https://doi.org/10.1083/jcb.200406049

663 Koláčková V, Perničková K, Vrána J, Duchoslav M, Jenkins G, Phillips D, Turkosi E,
664 Šamajová O, Sedlářová M, Šamaj J, Doležel J, Kopecký D. 2019. Nuclear disposition of alien
665 chromosome introgressions into wheat and rye using 3D-FISH. *International Journal of*

Molecular Sciences 20(17), 4143. https://doi.org/10.3390/ijms20174143

Kubalová I, Câmara AS, Cápal P, Beseda T, Rouillard JM, Krause GM, Holušová K, Toegelová H, Himmelbach A, Stein N, Houben A, Doležel J, Mascher M, Šimková H, Schubert V. 2023. Helical coiling of metaphase chromatids. *Nucleic Acids Research* 51(6), 2641-2654. https://doi.org/ 10.1093/nar/gkad028

Levi V, Ruan Q, Plutz M, Belmont AS, Gratton E. 2005. Chromatin dynamics in interphase cells revealed by tracking in a two-photon excitation microscope. *Biophysical Journal* 89(6), 4275-4285. https://doi.org/10.1529/biophysj.105.066670

Lieberman-Aiden E, van Berkum NL, Williams L, Imakaev M, Ragoczy T, Telling A, Amit I, Lajoie BR, Sabo PJ, Dorschner MO, Sandstrom R, Bernstein B, Bender MA, Groudine M, Gnirke A, Stamatoyannopoulos J, Mirny LA, Lander ES, Dekker J. 2009. Comprehensive mapping of long-range interactions reveals folding principles of the human genome. *Science* 326, 289–293. https://doi.org/10.1126/science.1181369

Liu C, Cheng YJ, Wang JW, Weigel D. 2017. Prominent topologically associated domains differentiate global chromatin packing in rice from *Arabidopsis*. *Nature Plants* 3(9), 742-748. https://doi.org/10.1038/s41477-017-0005-9

Liu X, Sun S, Wu Y, Zhou Y, Gu S, Yu H, Yi C, Gu M, Jiang J, Liu B, Zhang T, Gong Z. 2020. Dual-color oligo-FISH can reveal chromosomal variations and evolution in *Oryza* species. *Plant Journal* 101(1), 112-121. https://doi.org/10.1111/tpj.14522

Lysák MA, Fransz PF, Ali HB, Schubert I. 2001. Chromosome painting in *Arabidopsis thaliana*. *Plant Journal* 28(6):689–97. https://doi.org/10.1046/j.1365-313x.2001.01194.x

Maeshima K, Ide S, Babokhov M. 2019. Dynamic chromatin organization without the 30-nm fiber. *Current Opinion in Cell Biology* 58, 95-104. https://doi.org/10.1016/j.ceb.2019.02.003

Markaki Y, Smeets D, Fiedler S, Schmid VJ, Schermelleh L, Cremer T, Cremer M. 2012. The potential of 3D-FISH and super-resolution structured illumination microscopy for studies of 3D nuclear architecture: 3D structured illumination microscopy of defined chromosomal structures visualized by 3D (immuno)-FISH opens new perspectives for studies of nuclear architecture. *BioEssays*: news and reviews in molecular, cellular and developmental biology. 34:412–426. https://doi.org/10.1002/bies.201100176

Matsuda A, Shao L, Boulanger J, Kervrann C, Carlton PM, Kner P, Agard D, Sedat JW. 2010. Condensed mitotic chromosome structure at nanometer resolution using PALM and EGFP-

histones. *PloS One* 5(9), e12768. https://doi.org/10.1371/journal.pone.0012768

Misteli T. 2020. The self-organizing genome: principles of genome architecture and function. *Cell* 183(1), 28-45. https://doi.org/10.1016/j.cell.2020.09.014

Moors TE, Maat CA, Niedieker D, Mona D, Petersen D, Timmermans-Huisman E, Kole J, El-Mashtoly SF, Spycher L, Zago W, Barbour R, Mundigl O, Kaluza K, Huber S, Hug MN, Kremer T, Ritter M, Dziadek S, Geurts JJG, Gerwert K, Britschgi M, van de Berg WDJ. 2021. The subcellular arrangement of alpha-synuclein proteoforms in the Parkinson's disease brain as revealed by multicolor STED microscopy. *Acta Neuropathologica* 142, 423-448. https://doi.org/10.1007/s00401-021-02329-9

Nagano T, Lubling Y, Stevens TJ, Schoenfelder S, Yaffe E, Dean W, Laue E, Tanay A, Fraser P. 2013. Single-cell Hi-C reveals cell-to-cell variability in chromosome structure. *Nature* 502(7469), 59-64. https://doi.org/10.1038/nature12593

Němečková A, Koláčková V, Vrána J, Doležel J, Hřibová E. 2020. DNA replication and chromosome positioning throughout the interphase in three-dimensional space of plant nuclei. *Journal of Experimental Botany* 71(20), 6262-6272. https://doi.org/10.1093/jxb/eraa370

Nozaki T, Imai R, Tanbo M, Nagashima R, Tamura S, Tani T, Joti Y, Tomita M, Hibino K, Kanemaki MT, Wendt KS, Okada Y, Nagai T, Maeshima K. 2017. Dynamic organization of chromatin domains revealed by super-resolution live-cell imaging. *Molecular Cell* 67(2), 282-293. https://doi.org/10.1016/j.molcel.2017.06.018

Nozaki T, Shinkai S, Ide S, Higashi K, Tamura S, Shimazoe MA, Nakagawa M, Suzuki Y, Okada Y, Sasai M, Onami S, Kurokawa K, Iida S, Maeshima K. 2023. Condensed but liquid-like domain organization of active chromatin regions in living human cells. *Science Advances* 9(14), eadf1488. https://doi.org/10.1126/sciadv.adf1488

Ohmido N and Fukui K. 1995. Cytological studies of African cultivated rice, *Oryza glaberrima*. *Theoretical and Applied Genetics* 91(2), 212-217. https://doi.org/10.1007/BF00220880

Pečinka A, Schubert V, Meister A, Kreth G, Klatte M, Lysák MA, Fuchs J, Schubert I. 2004. Chromosome territory arrangement and homologous pairing in nuclei of *Arabidopsis thaliana* are predominantly random except for NOR-bearing chromosomes. *Chromosoma* 113, 258–269. https://doi.org/ 10.1007/s00412-004-0316-2

Perničková K, Koláčková V, Lukaszewski AJ, Fan C, Vrána J, Duchoslav M, Jenkins G, Phillips D, Šamajová O, Sedlářová M, Šamaj J, Doležel J, Kopecký D. 2019. Instability of alien chromosome introgressions in wheat associated with improper positioning in the nucleus. I*nternational Journal of Molecular Sciences* 20(6), 1448. https://doi.org/10.3390/ijms20061448

Pontvianne F, Blevins T, Chandrasekhara C, Mozgová I, Hassel C, Pontes OM, Tucker S, Mokros P, Muchová V, Fajkus J, Pikaard CS. 2013. Subnuclear partitioning of rRNA genes between the nucleolus and nucleoplasm reflects alternative epiallelic states. *Genes & Development* 27(14), 1545-1550. https://doi.org/10.1101/gad.221648.113

Prieto EI and Maeshima K. 2019. Dynamic chromatin organization in the cell. *Essays in Biochemistry* 63(1), 133-145. https://doi.org/10.1042/EBC20180054

Prieto P, Shaw P, Moore G. 2004. Homologue recognition during meiosis is associated with a change in chromatin conformation. *Nature Cell Biology* 6, 906. https://doi.org/ 10.1038/ncb1168

Rabl C. 1885. Uber Zelltheilung. Morphologisches Jahrbuch 10, 214–330.

Ramani V, Deng X, Qiu R, Gunderson KL, Steemers FJ, Disteche CM, Noble WS, Duan Z, Shendure J. 2017. Massively multiplex single-cell Hi-C. *Nature Methods*, 14(3), 263-266. https://doi.org/10.1038/nmeth.4155

Ramírez F, Bhardwaj V, Arrigoni L, Lam KC, Grüning BA, Villaveces J, Habermann B, Akhtar A, Manke T. 2018. High-resolution TADs reveal DNA sequences underlying genome organization in flies. *Nature Communications* 9(1), 189. https://doi.org/10.1038/s41467-017-02525-w

Robaszkiewicz E, Idziak-Helmcke D, Tkacz MA, Chrominski K, Hasterok R. 2016. The arrangement of Brachypodium distachyon chromosomes in interphase nuclei. *Journal of Experimental Botany* 67(18), 5571-5583. https://doi.org/10.1093/jxb/erw325

Santos AP and Shaw P. 2004. Interphase chromosomes and the Rabl configuration: does genome size matter?. *Journal of Microscopy* 214, 201-206. https://doi.org/10.1111/j.0022-2720.2004.01324.x

Sexton T and Cavalli G. 2015. The role of chromosome domains in shaping the functional genome. *Cell* 160(6), 1049-1059. https://doi.org/10.3390/ijms21103488

Shan W, Kubová M, Mandáková T, Lysak MA. 2021. Nuclear organization in crucifer

759 genomes: nucleolus-associated telomere clustering is not a universal interphase configuration
760 in Brassicaceae. *Plant Journal* 108(2), 528-540. https://doi.org/10.1111/tpj.15459

761 Szabo Q, Jost D, Chang JM, Cattoni DI, Papadopoulos GL, Bonev B, Sexton T, Gurgo J,
762 Jacquier C, Nollmann M, Bantignies F, Cavalli G.2018. TADs are 3D structural units of
763 higher-order chromosome organization in Drosophila. *Science Advances* 4: eaar8082.
764 https://doi.org/10.1126/sciadv.aar8082

765 Tan L Xing D Chang CH, Li H, Xie XS. 2018. Three-dimensional genome structures of single
766 diploid human cells. *Science* 361(6405), 924-928. https://doi.org/10.1126/science.aat5641

767 Tiku V and Antebi A. 2018. Nucleolar function in lifespan regulation. *Trends in Cell*
768 *Biology* 28(8), 662-672. https://doi.org/10.1016/j.tcb.2018.03.007

769 Tulpová Z, Kovařík A, Toegelová H, Navrátilová P, Kapustová V, Hřibová E, Vrána J, Macas
770 J, Doležel J, Šimková H. 2022. Fine structure and transcription dynamics of bread wheat
771 ribosomal DNA loci deciphered by a multi-omics approach. *Plant Genome* 15(1), e20191.
772 https://doi.org/10.1002/tpg2.20191

773 Valli J, Garcia-Burgos A, Rooney LM, e Oliveira BVDM, Duncan RR, Rickman C. 2021.
774 Seeing beyond the limit: a guide to choosing the right super-resolution microscopy
775 technique. *Journal of Biological Chemistry* 297(1).https://doi.org/10.1016/j.jbc.2021.100791

776 Wang C, Liu C, Roqueiro D, Grimm D, Schwab R, Becker C, Lanz Ch, Weigel D. 2015.
777 Genome-wide analysis of local chromatin packing in *Arabidopsis thaliana*. *Genome*
778 *Research* 25(2), 246-256. https://doi.org/10.1101/gr.170332.113

779 Woodcock CL, Frado LL, Rattner JB. 1984. The higher-order structure of chromatin:
780 evidence for a helical ribbon arrangement. *Journal of Cell Biology* 99(1),
781 42-52.https://doi.org/10.1083/jcb.99.1.42

782 Zhang T, Liu G, Zhao H, Braz GT, Jiang J. 2021. Chorus2: design of genome-scale
783 oligonucleotide-based probes for fluorescence in situ hybridization. *Plant Biotechnology*
784 *Journal* 19(10), 1967-1978. https://doi.org/doi: 10.1111/pbi.13610

785 Zhou S, Jiang W, Zhao Y, Zhou DX. 2019. Single-cell three-dimensional genome structures
786 of rice gametes and unicellular zygotes. *Nature Plants* 5(8), 795-800. https://doi.org/
787 10.1038/s41477-019-0471-3

788

Legends to figures

Table 1

Analysis of all tested G1 nuclei specific for both analyzed tissues revealing variation in shape and volume of nucleus and nucleolus.

Table 2

Characteristics of analyzed G1 nuclei and CTs.

Table 3

Analysis of G1 nuclei and 45s rDNA.

Figure 1

Chromatin condensation in G1 nuclei of young leaves and root meristem. DNA was stained by spirochrome (white). Differences in DNA structure are clearly visible in zoomed pictures and heat maps (A). (B) Graph of chromatin fiber width measurement. Bar 2 µm.

Figure 2

Representative figures of oligo-painting FISH and immunolabeling. (A) Differences in shape of analyzed nuclei (nuclear DNA stained by DAPI, blue). Nucleolus was visualized using fibrillarin immunolabeling (red). (B) Correlation between shape of the nucleus and CTs association. (C) Visualization of centromere (yellow), short arm of chromosome 2 (2S) (pink), and long arm (2L) (green) on metaphase chromosomes. (D) Visualization of chromosome 2 (pink) and chromosome 9 (green) by oligo-painting FISH on prometaphase chromosomes. Chromosomes were counterstained with DAPI (blue). (E) Maximal intensity projection of G1 nuclei. Two separate chromosome territories correspond to two homologues chromosomes. Long arm (2L) of chromosome in pink, short arm of chromosome (2S) in yellow. DNA was counterstained with DAPI (blue). Bar 3 µm.

Figure 3

Maximal intensity projection of G1 nuclei of rice with immuno-FISH localization of different specific probes on flow sorted G1 nuclei of root meristem (A, C, D) and leaf tissue (B). DNA was counterstained with DAPI (blue). Bar 2 µm.

Figure 4

Comparison between root and leaf chromosome arrangement. (A) Models of individual arrangements created with BioRender.com. based on raw data observation. (B) Graph of both chromosome association comparison. Association and separation in displayed in root and leaf tissue.

Figure 5

3D models of CTs positioning in root and leave G1 nuclei. (A) Spatial positioning of CTs specific to chromosome 2 (yellow) and 9 (green) and nucleoli (red). (B) Model showing spatial arrangement of the CTs and nucleoli with respect to the center and periphery of the nucleus.
Shells of equal area depict regions of the nuclei, where signals of DAPI (white) and chromosome 2 (yellow) and chromosome 9 (green) were localized.

Figure 6

Oligo-painting FISH on root ultra-thin sections prepared by cryomicrotome. Centromeric probe (red), telomeric probe (green) and specific probe for chromosome 2 (yellow) were applied. Pictures displayed evidence of Rabl configuration in xylem (A) and in cortex (B) cells.

Supplemental data

Supplementary Figure 1

Differences in chromosome 9 arrangement (green) and 45s rDNA (yellow) activity in root and leaf. Models of individual arrangements were created based on raw data observation using BioRender.com.

Supplementary Video 1

Rice root nucleus in G1 phase. Chromosome 2 (yellow) and chromosome 9 (green) were visualized using oligo-painting FISH. Nucleolus was stained by immunolabeling with fibrillarin (red). Nuclear DNA was counterstained with DAPI (blue)

Supplementary Video 2

Rice leaf nucleus in G1 phase. Chromosome 2 (yellow) and chromosome 9 (green) were

857 visualized using oligo-painting FISH. Nucleolus was stained by immunolabeling fibrillarin
858 (red). Nuclear DNA was counterstained with DAPI (blue)

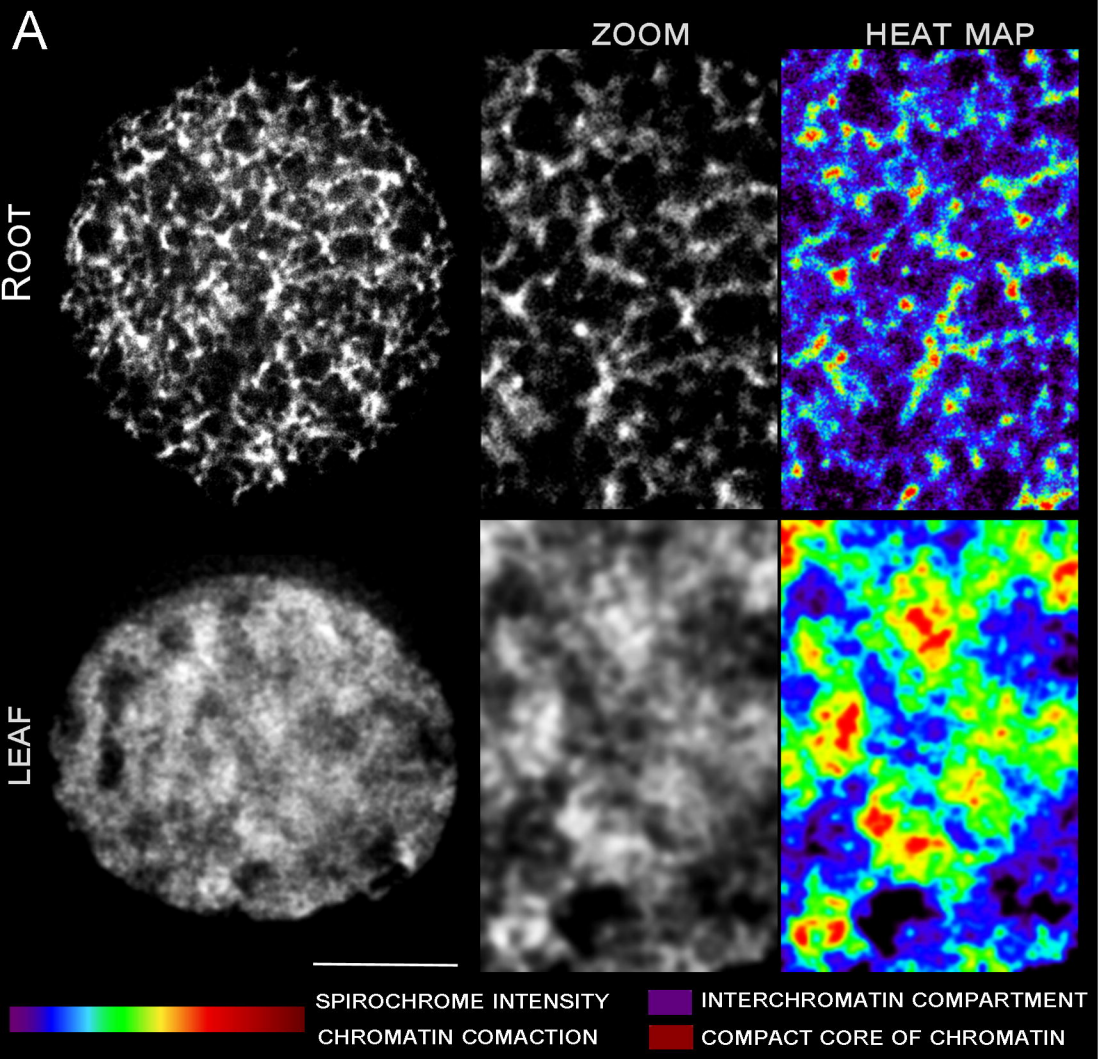
A
ZOOM
HEAT MAP
ROOT
LEAF
SPIROCHROME INTENSITY
CHROMATIN COMACTION
INTERCHROMATIN COMPARTMENT
COMPACT CORE OF CHROMATIN

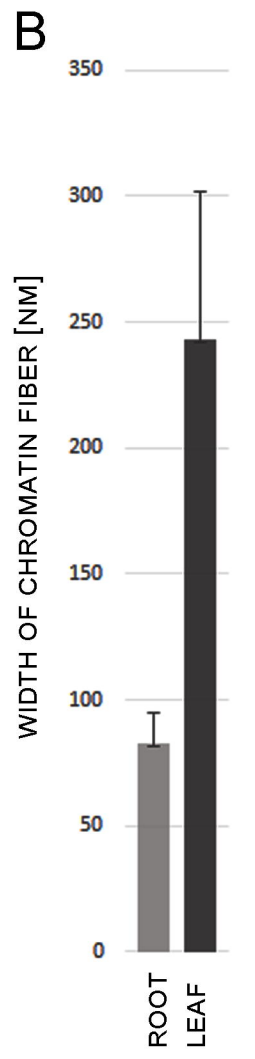
B
WIDTH OF CHROMATIN FIBER [NM]
350
300
250
200
150
100
50
0
ROOT
LEAF

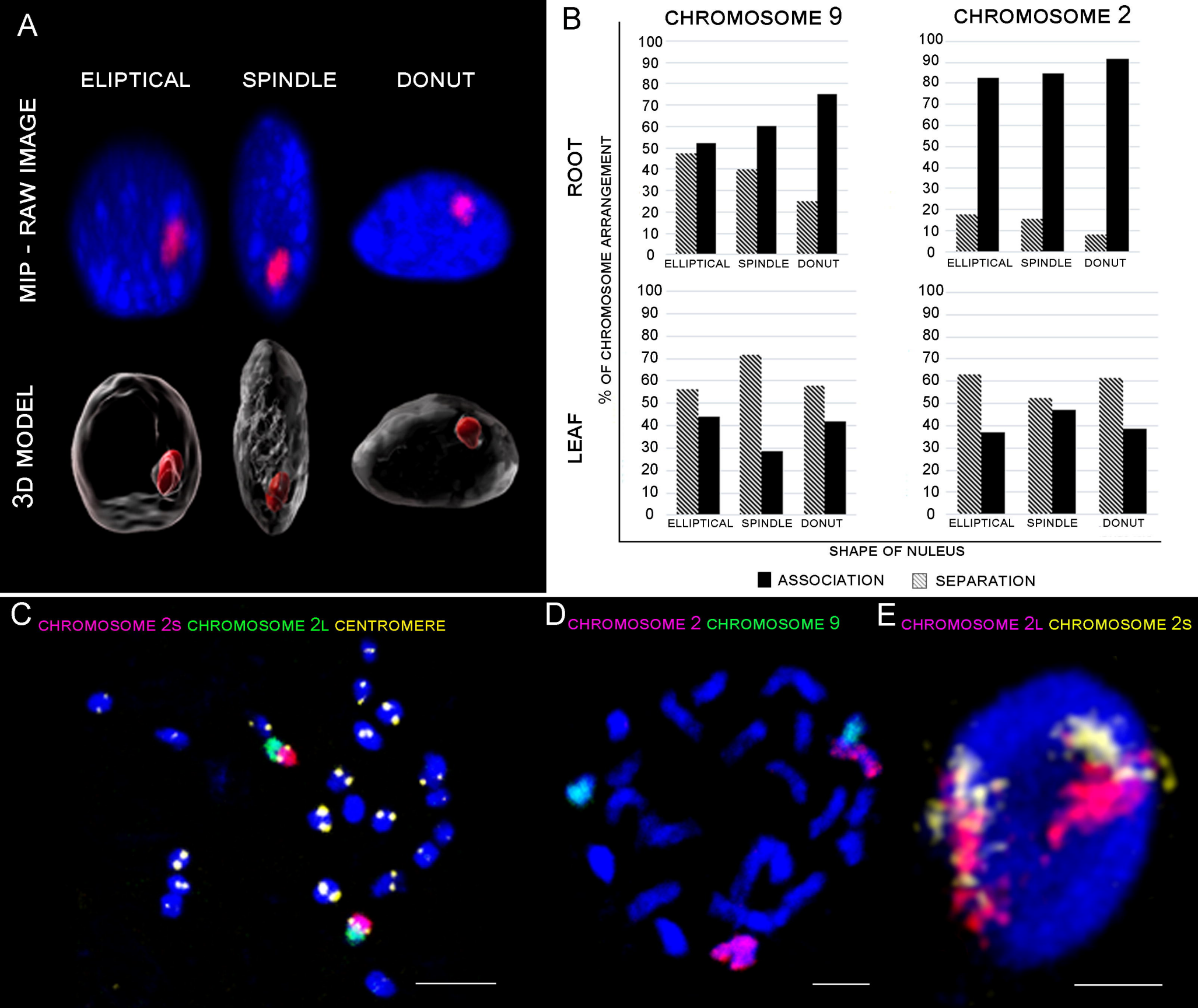
A
ELIPTICAL
SPINDLE
DONUT
MIP - RAW IMAGE
3D MODEL
B
CHROMOSOME 9
CHROMOSOME 2
ROOT
LEAF
% OF CHROMOSOME ARRANGEMENT
100
90
80
70
60
50
40
30
20
10
0
ELLIPTICAL
SPINDLE
DONUT
SHAPE OF NULEUS
ASSOCIATION
SEPARATION
C
CHROMOSOME 2S CHROMOSOME 2L CENTROMERE
D
CHROMOSOME 2 CHROMOSOME 9
E
CHROMOSOME 2L CHROMOSOME 2S

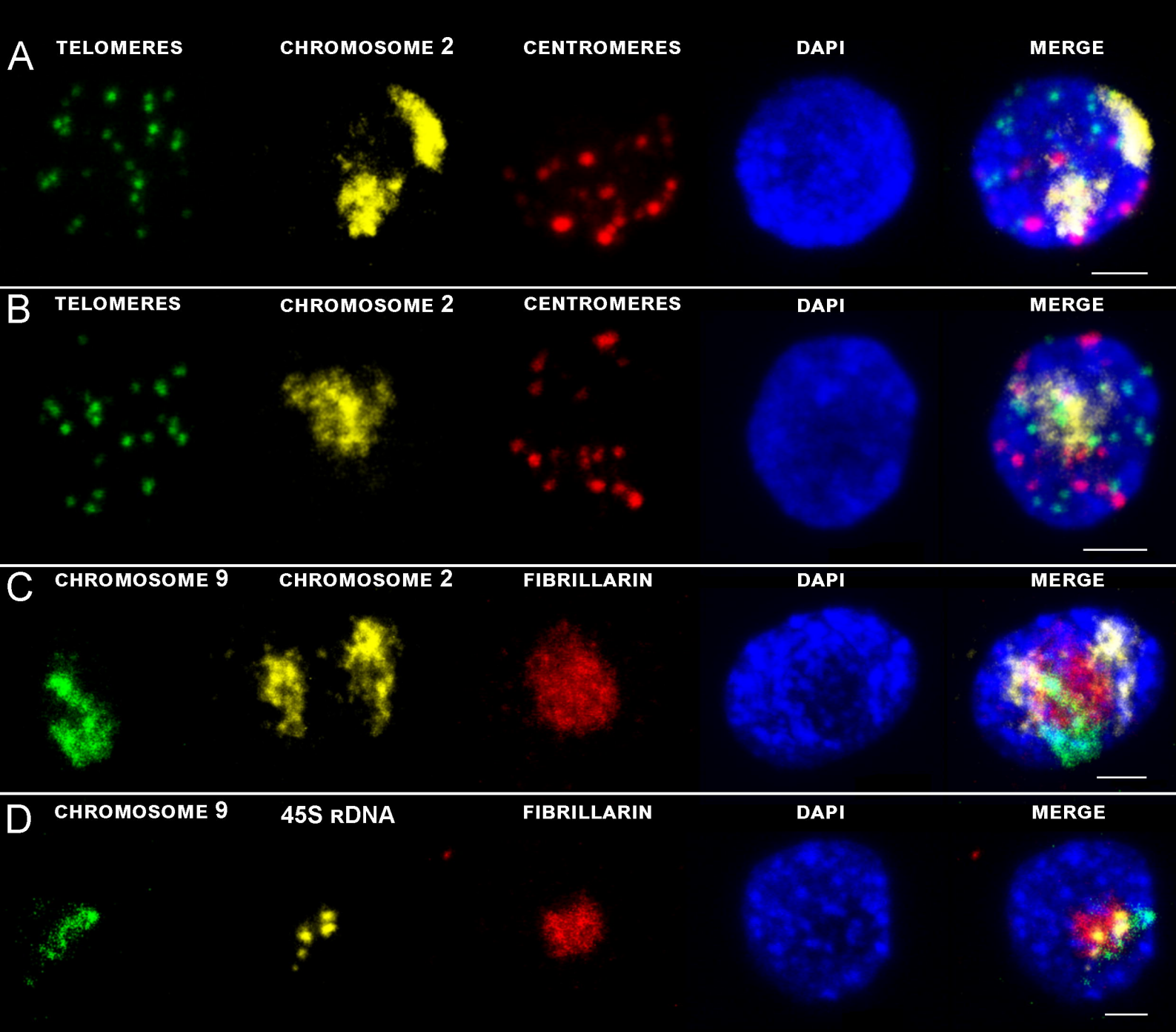
A
TELOMERES
CHROMOSOME 2
CENTROMERES
DAPI
MERGE
B
TELOMERES
CHROMOSOME 2
CENTROMERES
DAPI
MERGE
C
CHROMOSOME 9
CHROMOSOME 2
FIBRILLARIN
DAPI
MERGE
D
CHROMOSOME 9
45S rDNA
FIBRILLARIN
DAPI
MERGE

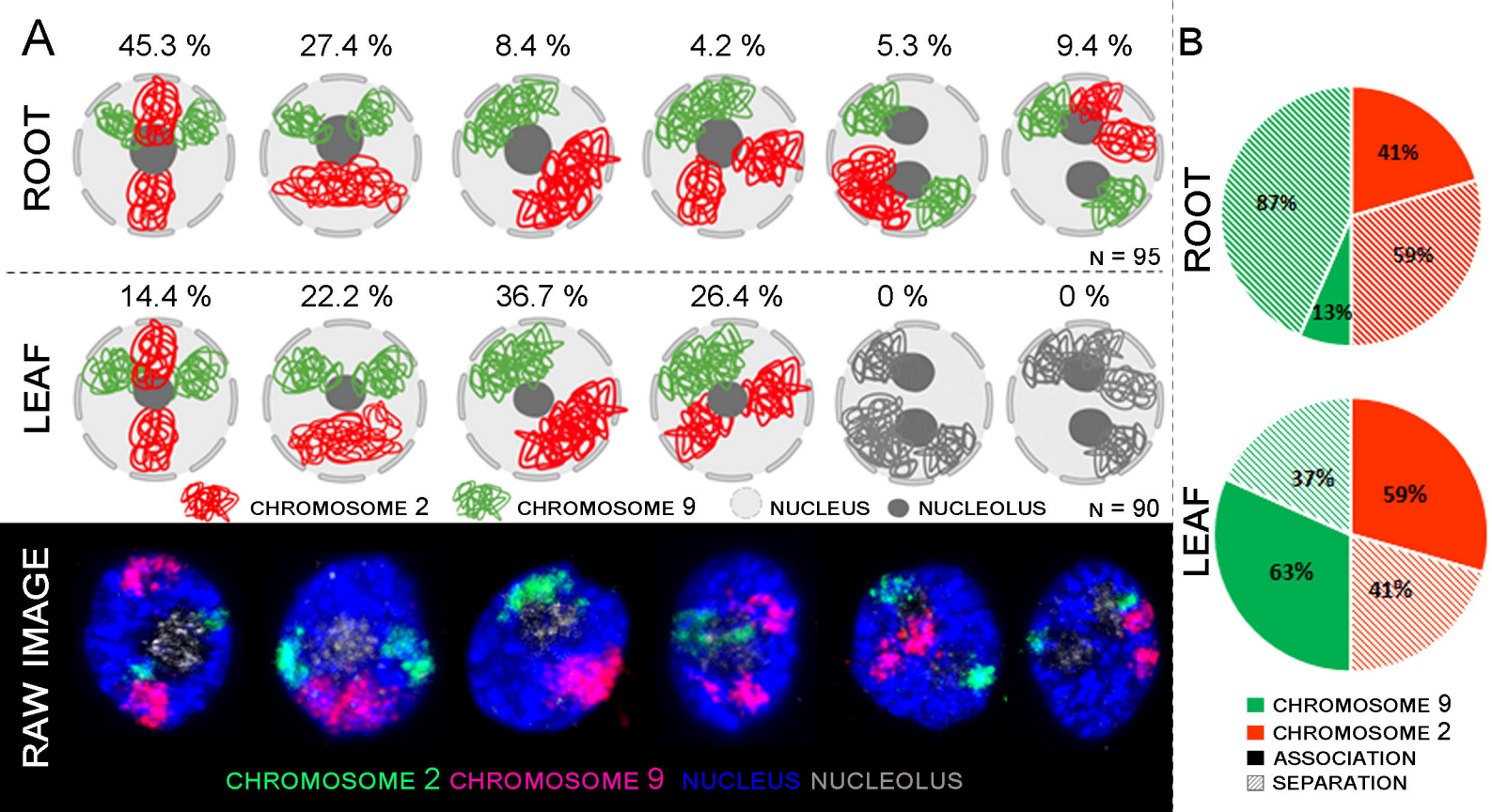
A
ROOT
45.3 %
27.4 %
8.4 %
4.2 %
5.3 %
9.4 %
N = 95
LEAF
14.4 %
22.2 %
36.7 %
26.4 %
0 %
0 %
CHROMOSOME 2
CHROMOSOME 9
NUCLEUS
NUCLEOLUS
N = 90
RAW IMAGE
CHROMOSOME 2 CHROMOSOME 9 NUCLEUS NUCLEOLUS
B
ROOT
87%
41%
59%
13%
LEAF
37%
59%
63%
41%
CHROMOSOME 9
CHROMOSOME 2
ASSOCIATION
SEPARATION

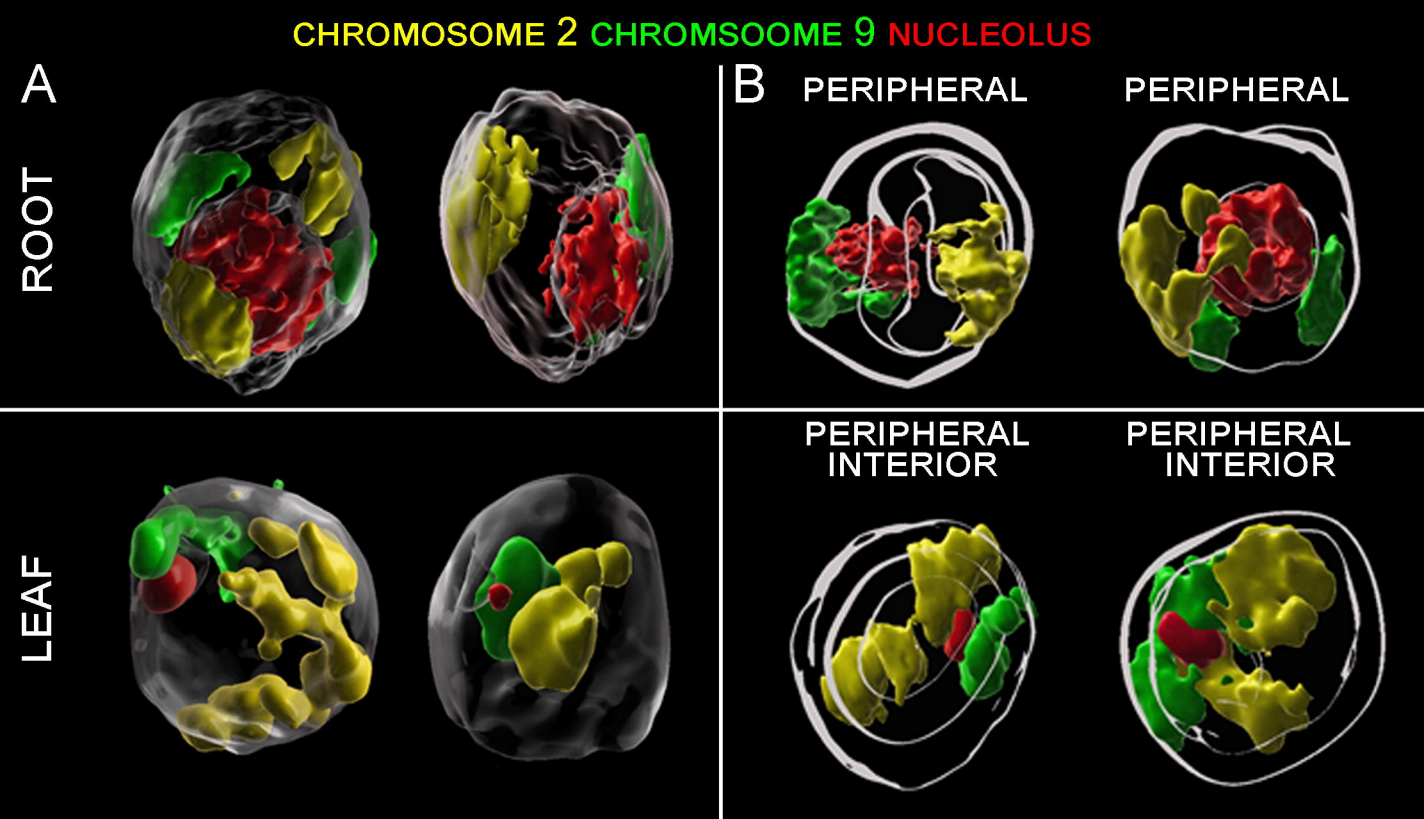
CHROMOSOME 2 CHROMSOOME 9 NUCLEOLUS
A
ROOT
B
PERIPHERAL
PERIPHERAL
LEAF
PERIPHERAL INTERIOR
PERIPHERAL INTERIOR

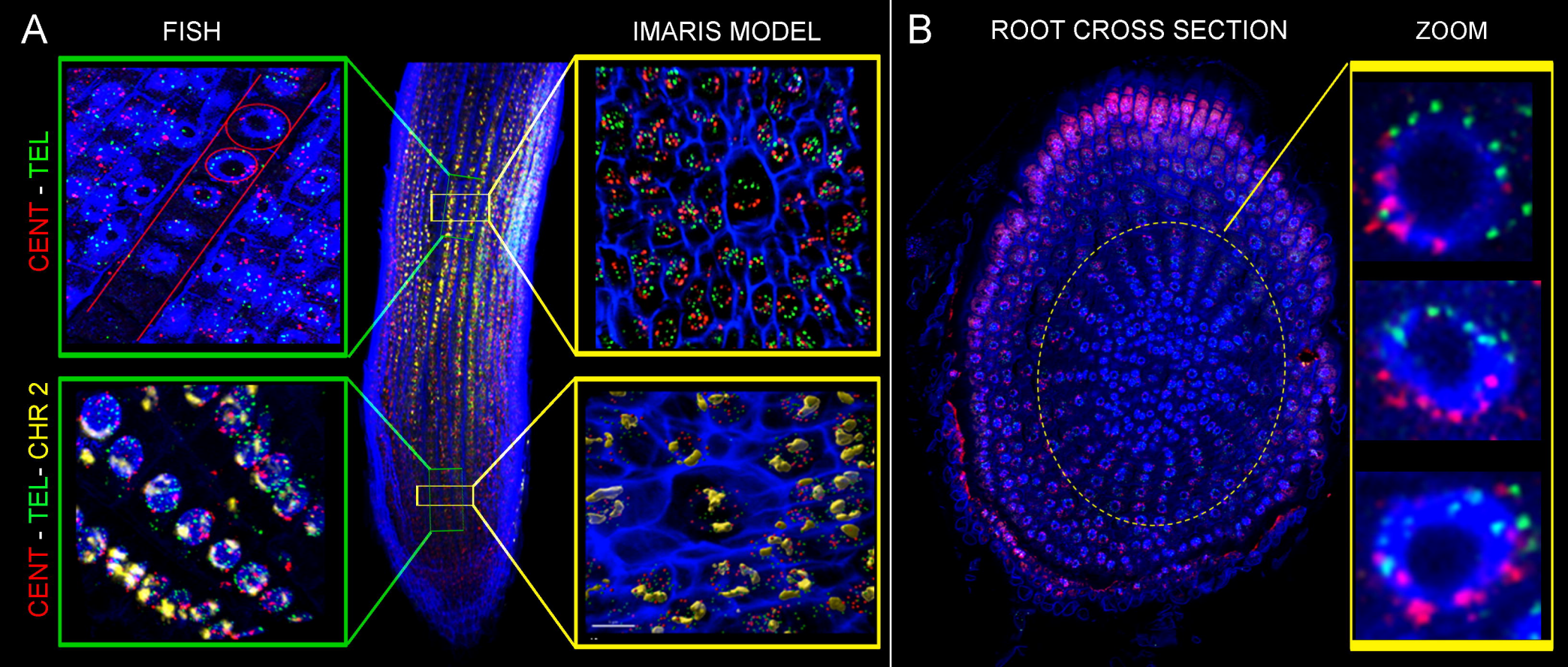
A
FISH
IMARIS MODEL
CENT - TEL
CENT - TEL- CHR 2
B
ROOT CROSS SECTION
ZOOM